QUANTITATIVE SIMULATION OF ENDPLATE CURRENTS AT NEUROMUSCULAR JUNCTIONS BASED ON THE REACTION OF ACETYLCHOLINE WITH ACETYLCHOLINE RECEPTOR AND ACETYLCHOLINESTERASE

TERRONE L. ROSENBERRY, *Departments of Biochemistry and Neurology, College of Physicians and Surgeons, Columbia University, New York 10032 U.S.A.*

ABSTRACT Two kinetic models are introduced which predict amplitudes and time-courses of endplate currents and miniature endplate currents at neuromuscular junctions, at both normal and acetylcholinesterase-inhibited endplates. Appropriate differential rate equations reflecting interactions of acetylcholine with acetylcholine receptor and with esterase, diffusion of acetylcholine both within and from the synaptic cleft, and cooperativity between receptor site occupancy and ion channel opening are solved. Acetylcholine release into the cleft is assumed to be instantaneous. The simpler homogeneous reaction space model accurately predicts decay phase time constants under a variety of conditions, but its predictions of amplitudes and growth phase time constants are inaccurate. The two-reaction space model predicts amplitudes and time constants within a factor of two of those observed experimentally. The simulations indicate that the amplitudes and time-courses are primarily determined by the chemical reaction rates that characterize acetylcholine interactions with receptor and esterase and that these interactions occur under nonequilibrium conditions. Approximately 50% of the total ion channels in the initial reaction space are predicted to be opened at the peak endplate current. The cooperative opening of ion channels by acetylcholine requires that acetylcholine be introduced into the cleft in discrete, concentrated elements. Virtually all the open channels are confined to the initial reaction space, although acetylcholine-bound receptor sites can be much more widely distributed.

INTRODUCTION

The characteristics of synaptic transmission at neuromuscular junctions have been intensively studied. The propagation of a nerve impulse into an axon terminal triggers a sequence of molecular events that produces transient ionic currents in the postsynaptic muscle membrane; these currents in turn lead to a propagating action potential in the muscle and a muscle twitch. The molecular events that give rise to the postsynaptic endplate currents (epcs) include the release of acetylcholine; its subsequent interaction with two membrane-bound proteins, acetylcholine receptor and acetylcholinesterase; and a consequent conductance increase involving specific ion channels in the postsynaptic membrane. A neurotransmitter theory of acetylcholine action has been formulated by Katz and his colleagues (Katz, 1969) to describe these molecular events, and this theory has obtained wide experimental support (Steinbach and Stevens, 1976). Despite this agreement, no quantitative treatment has yet been introduced to account for the amplitudes and the time-course of epcs in terms of the kinetic

rate constants that characterize the reaction of acetylcholine with receptor and esterase. Two difficulties have hampered the development of such a treatment. First, estimates of all the appropriate kinetic rate constants have become available only in the past two years; second, somewhat arbitrary approximations regarding the geometry, topology, and homogeneity of the reaction space within the synapse are required to derive the mathematical formalism. Assumptions sufficient to overcome these difficulties and to permit epc simulations are described in this report.

The task of simulating epcs is a formidable one. A major objective of this report is to introduce a kinetic framework for the analysis of acetylcholine action at synapses. Simple kinetic models will be constructed that permit the solution of appropriate differential equations. When values of kinetic constants estimated entirely independently of nerve-evoked epc phenomena are inserted into these equations, a reasonable simulation of these phenomena is achieved. It is possible that more elaborate kinetic models or revised kinetic constant estimates may necessitate insertion of additional differential equations or revision of the simulation profiles in the future. However, the present theoretical treatment is intended to be sufficiently comprehensive to permit several interesting conclusions about the dynamics of acetylcholine action in the synapse.

Several factors limit the accuracy and precision of epc simulations. Morphological features of neuromuscular junctions vary both among muscles and among species; the reaction rate constants of some of the critical chemical reactions are estimated only to within a factor of two; and electrophysiological measurements which provide the criteria for the quality of the epc simulations show some variability in reported values. Consequently, a major assumption in this formulation is that the properties of an idealized synapse which is constructed with morphological data taken largely from rat diaphragm junctions and with chemical reaction constant data from both solubilized and intact electric organ preparations can be compared with electrophysiological data from amphibian endplates. Considerable data support such an interspecies amalgamation at the level required for the simulations.

Description of mepc and epc Phenomena

The epc simulations in this report assume that epcs are a linear summation of miniature endplate currents (mepcs) which arise from the release of acetylcholine into the synaptic cleft reaction space. Acetylcholine release is assumed to be instantaneous relative to the time-course of mepcs. The simulations replicate the experimentally measured growth- and decay-phase time constants and normalized amplitudes of the typical mepcs shown in Fig. 1, both in the normal synapse and after total esterase inhibition. The normalized amplitudes in the epc simulations are expressed as the ratio of the number of open ion channels to the total number of released acetylcholine molecules. The relationship between the magnitude of an mepc or an epc and the corresponding number of open ion channels is well defined experimentally (Katz and Miledi, 1972; Anderson and Stevens, 1973) and leads to estimates that the maximum number of open ion channels at peak mepcs or epcs is about 10% of the total number of acetylcholine molecules released, either in frog or in rat junctions (see Colquhoun, 1975). The growth time (time for an mepc to increase from 20 to 80% of its maximum amplitude; Gage and McBurney, 1975) associated with the study in Fig. 1 is quite variable but averages about 120 μs, a value similar to that seen for mepcs in eel electroplax

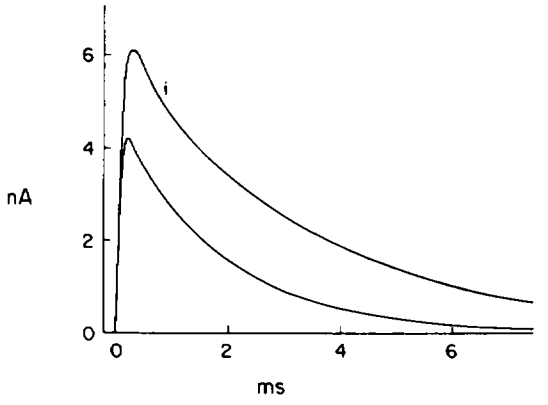

FIGURE 1 Experimentally recorded mepcs in the toad neuromuscular junction (redrawn from Gage and McBurney, 1975). Recordings were made in a single voltage-clamped fiber in standard Ringer solution and correspond to a clamp potential of −70 mV and a temperature of 25°C. The upper trace (i) was recorded after a 30-min exposure to 3 μM neostigmine in Ringer solution, a condition assumed to completely inhibit esterase without effect on receptor (but see footnote 1).

(see Lester et al., 1978). The decay phase is very sensitive both to temperature and to the postsynaptic membrane voltage. The decay is exponential and, under the conditions in Fig. 1, is characterized by a reciprocal time constant of $6 \times 10^2\ s^{-1}$. Similar values are observed for both mepc and epc decays in frog junctions ($5 \times 10^2\ s^{-1}$; Anderson and Stevens, 1973) and for epc decays in eel electrophax ($16 \times 10^2\ s^{-1}$; Sheridan and Lester, 1977). After esterase inhibition, relative amplitudes increase about 1.5-fold for mepcs in Fig. 1 and about 2-fold for epcs in frog junctions[1] (Takeuchi and Takeuchi, 1959; Kordas, 1972*b*); the growth time for mepcs in Fig. 1 is reported to show little or no increase (Gage and McBurney, 1975), although the time to peak amplitude for epcs in frog junctions increases about 1.7-fold (Takeuchi and Takeuchi, 1959; Magleby and Stevens, 1972*a*), and the decay phase time constant is prolonged from two- or three-fold (Takeuchi and Takeuchi, 1959; Magleby and Stevens, 1972*a*; Gage and McBurney, 1975; Sheridan and Lester, 1977) to about four-fold (Kordas, 1972*b*; Katz and Miledi, 1973; Magleby and Terrar, 1975).

Construction of Synapse Models Which Lead to epc Simulations

The structure of the idealized synapse considered here is schematized in Fig. 2. The following quantitative features, taken for rat diaphragm, are important to the simulations. In addition to the value of the transverse length l, which is discussed in later sections, the synaptic cleft width w is taken as 0.05 μm and the total synaptic cleft volume, V, as 450 μm^3 (Salpeter and Eldefrawi, 1973). The total number of synaptic receptor sites, R^0, which bind acetylcholine is assumed to be 2×10^7, one-half (Raftery et al., 1976; Chang and Bock, 1977; Damle and Karlin, 1978) the total number of α-bungarotoxin binding sites (Miledi and Potter, 1971; Fambrough and Hartzell, 1972). The total number of acetylcholinesterase sites, E^0, is also

[1]A somewhat smaller relative increase in amplitude is observed when neostigmine is used to block esterase, presumably because typical neostigmine concentrations even of 3 μM have a slight curarelike effect and block a small fraction of receptor sites (Magleby and Stevens, 1972*a*; Katz and Miledi, 1973; Magleby and Terrar, 1975).

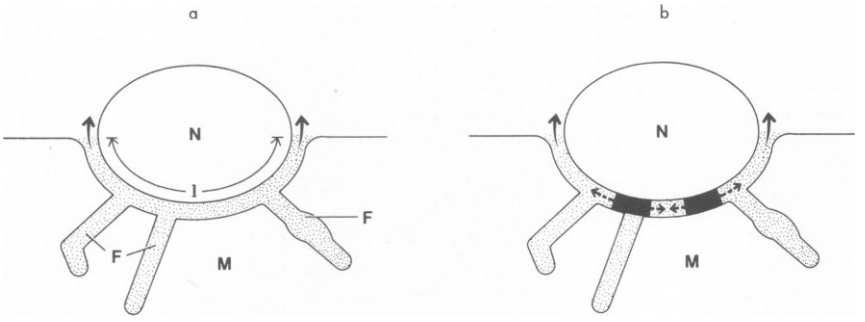

FIGURE 2 Schematic structure of an idealized neuromuscular junction. The nerve terminal (N) lies in a shallow primary fold of the muscle (M) to form a synapse shown in cross section with a transverse length l. The longitudinal length of the synapse is presumed to be several times l. Numerous secondary junctional folds (F) occur as infoldings of the muscle membrane and are shown here as tubular cleft projections characteristic of rat and mouse diaphragm junctions (see, for example, Salpeter and Eldefrawi, 1973). Secondary folds in frog junctions are shallower and appear as troughs running perpendicular to the longitudinal axis of the primary fold (see Steinbach and Stevens, 1976). (*a*) Homogeneous reaction space model. Acetylcholine, receptor, and esterase are distributed homogeneously in the synaptic reaction space indicated by the stippled area. Acetylcholine diffuses out of the synaptic cleft only at the transverse edges as indicated by the arrows. (*b*) Two-reaction space model. Acetylcholine is initially present only in discrete reaction space elements shaped essentially like flattened cylinders between pre- and postsynaptic membranes in the primary fold (solid areas are sections of such elements parallel to their cylindrical axes). Acetylcholine diffuses into the remainder of the synaptic cleft only by radial diffusion through the cylindrical surface of each element (dashed arrows). Esterase is homogeneously distributed throughout the synaptic cleft, but receptor is more concentrated in the cylindrical elements. Although the concentrations of both acetylcholine and receptor thus differ between the two-reaction spaces, both species are assumed to be distributed homogenously within each reaction space at all times.

assumed to be 2×10^7 (Barnard et al., 1971). Estimates of w, V, R^0, and E^0 for frog junctions are within a factor of two of these values (Porter et al., 1973; Steinbach and Stevens, 1976).

A useful initial model for the epc simulations is to assume that acetylcholine, receptor, and esterase are distributed homogeneously throughout the synaptic reaction space at all times, as indicated in Fig. 2 *a*. Although this homogeneous reaction space model can account for epc decay rates under a variety of conditions, it is unable to simulate all the epc characteristics noted above. It does provide a necessary background for a more complicated two-reaction space model, shown in Fig. 2 *b*, which simulates the mepcs in Fig. 1 with reasonable accuracy. An important feature of the homogeneous reaction space model arises from the measured amount of total acetylcholine, A^0, released during an epc in rat diaphragm. This A^0 value of about 4×10^6 molecules (Mitchell and Krnjević, 1961; Potter, 1970) is only one-fifth of either the R^0 or E^0 values cited above. As a consequence of this overall stoichiometric excess of R^0 and E^0 over A^0, precise mathematical solutions to the appropriate chemical reaction rate equations can be obtained. The chemical schemes and rate constants required for the simulations are introduced in following sections, and techniques used for rate constant measurements have been reviewed elsewhere (Neumann et al., 1978). However, one rate constant merits special note. An overall bimolecular reaction rate constant, k_R, for acetylcholine reaction with receptor has been estimated recently both by biochemical techniques on the isolated torpedo receptor ($k_R = 2 \times 10^7\ M^{-1}\ s^{-1}$; Neumann and Chang, 1976; also see Grünhagen et al., 1977) and from electrophysiological measurements on eel electroplax cells

($k_R = 10^7\ M^{-1}\ s^{-1}$; Sheridan and Lester, 1977). These k_R estimates are about an order of magnitude smaller than the corresponding rate constant, k_E, for acetylcholine reaction with esterase, a discrepancy which at first glance appears to place receptor at a considerable competitive disadvantage relative to esterase for acetylcholine available in the synapse (see Neumann et al., 1978). This disadvantage in fact underlies the inadequacy of the homogeneous reaction space model in Fig. 2 *a*; to enable sufficient acetylcholine to interact with receptor, alternative models involving two-reaction spaces must be considered.

In brief, the two-reaction space model in Fig. 2 *b* is a somewhat arbitrary approximation of more precise multireaction space models that necessarily arise when acetylcholine is proposed to be spatially nonhomogeneous and thus can diffuse within the synaptic cleft. Acetylcholine is assumed initially to be confined homogeneously with juxtaneuronal reaction space elements from which it then diffuses into the remainder of the synaptic cleft. The quantitative features of such diffusion are considered in some detail later and are largely determined by the geometry of these reaction space elements and of the synaptic cleft itself. A second important facet of the two-reaction space model is a higher receptor concentration in the first reaction space elements. These higher receptor concentrations are indicated by higher juxtaneuronal densities corresponding to about 25,000–35,000 toxin sites/μm^2 of postsynaptic membrane in mouse and frog junctions (Fertuck and Salpeter, 1976; Matthews-Bellinger and Salpeter, 1978) and in eel electroplax (Bourgeois et al., 1972). The occurrence of a mepc is readily explained in the two-reaction space model as the spontaneous discharge of acetylcholine into a single first reaction space element, and the somewhat greater time to peak amplitude observed for epcs than for mepcs can be understood as arising from an asynchronous discharge of acetylcholine into several elements on arrival of a nerve impulse at the junction (Katz and Miledi, 1965). This formulation of the two-reaction space model thus is consistent with the proposal of vesicular acetylcholine release from the nerve terminal in the neurotransmitter theory of acetylcholine action (Katz, 1969). However, the model has been constructed with sufficient generality to permit, in principle, its application to a sequential model of acetylcholine interactions with excitable membranes (Neumann et al., 1973; Nachmansohn, 1959; see Neumann et al., 1978). This application also requires assumptions and cannot be investigated quantitatively until information about the location of esterase relative to receptor and details of the postulated separated reaction spaces are available.

REACTION SCHEMES

Acetylcholine Binding to Receptor

A two-state reaction scheme is generally considered to be a minimal model for acetylcholine interaction (see Colquhoun, 1975), and scheme I corresponds to such a model.

$$\begin{array}{ccc} A + R & \underset{k_{-1}}{\overset{k_1}{\rightleftharpoons}} & AR \\ k_c \,\big\uparrow\big\downarrow\, k_{-c} & & k_2 \,\big\uparrow\big\downarrow\, k_{-2} \\ A + R' & \underset{k'_{-1}}{\overset{k'_1}{\rightleftharpoons}} & AR' \end{array}$$

Scheme I

In scheme I, acetylcholine (A) binds to a receptor site in either its R or R' states. The R and AR species correspond to the closed or low conductance state, whereas the R' and AR' forms correspond to the open or high conductance state. The R and R' states interconvert by a protein conformation change as originally proposed by Nachmansohn (1955); and, in the presence of acetylcholine, the equilibria are shifted toward the open state. Similar schemes, some of which ignore the R' species, have been formulated previously (Del Castillo and Katz, 1957; Karlin, 1967; see Colquhoun, 1975).

Consider now the reduction of scheme I to the single overall equilibrium in scheme II. Such

$$A + R \underset{k_{-R}}{\overset{k_R}{\rightleftharpoons}} AR'$$

Scheme II

a reduction is suggested by two experimental systems. (a) Electrophysiological data indicate that perturbations of receptor-acetylcholine equilibria in eel electroplax (e.g., by voltage-jump of the clamped innervated membrane) result in epc relaxations that are characterized by a single exponential time-course (Sheridan and Lester, 1977). (b) Temperature-jump kinetic studies involving isolated torpedo receptor and acetylcholine show single exponential relaxations in the time range that corresponds to in vivo epcs (Neumann and Chang, 1976). In both systems, the concentration dependence of the observed relaxations is consistent with a bimolecular reaction like that in scheme II. The reduction of scheme I to scheme II could arise from several alternative physical situations. For example, if the species R' is negligible and AR and AR' equilibrate rapidly relative to the binding step $A + R \rightleftharpoons AR$, then k_R and k_{-R} are composite rate constants containing rate constant terms from reactions in scheme I (see Eigen and DeMaeyer, 1963; Sheridan and Lester, 1977). Alternatively, if R' and AR are present only at low concentration in a steady state and $R \rightarrow R'$ is not rate limiting for acetylcholine binding (i.e., $k_{-c} \gg k_1'[A]$, where square brackets indicate concentration), then the composite rate constants are given by $k_R = k_1k_2/(k_{-1} + k_2) + k_ck_1'/k_{-c}$ and $k_{-R} = k_{-1}k_{-2}/(k_{-1} + k_2) + k_{-1}'$. A physical situation assumed in other treatments (e.g., Magleby and Stevens, 1972b), that R' is negligible and that the binding equilibrium $A + R \rightleftharpoons AR$ is rapid relative to the equilibration of AR and AR', reduces to a slow equilibrium of unimolecular reactions. This situation could be modeled by a slight extension of the present treatment but would explicitly require the value of the rapid binding equilibrium constant, a constant for which no experimental evidence has yet been obtained.

Receptor Occupation and Ion Channel Opening

Early pharmacological observations suggested cooperativity in the opening of ion channels with respect to agonist concentration (see Rang, 1975). More recent studies support this suggestion and report Hill coefficients of nearly two, both for steady-state conductances in eel electroplax in the presence of acetylcholine or carbamylcholine (Lester et al., 1975; Sheridan and Lester, 1977) and in frog endplates with several agonists (Adams, 1975) and for transient epcs induced by iontophoretic application of these agonists to snake muscle endplates (Hartzell et al., 1975; Kuffler and Yoshikami, 1975). Slightly higher Hill coefficients are observed for these agonists applied iontophoretically to frog muscle endplates (Peper et al., 1976). Cooperativity could arise either in the binding of agonist to oligomeric units (Karlin,

1967; Changeux et al., 1967) or from a requirement of more than one occupied receptor site to open one ion channel (see Rang, 1975). The second alternative is assumed here and is supported by epc relaxation data on eel electroplax (Sheridan and Lester, 1977). These data suggest that ion channel opening occurs only when a second agonist molecule binds to a channel-receptor assembly but that agonist binding is not cooperative. Scheme III is one model that summarizes this proposal.

$$2A + R_2 \underset{k_{-R}}{\overset{2k_R}{\rightleftharpoons}} A + AR'R \underset{2k_{-R}}{\overset{k_R}{\rightleftharpoons}} A_2R_2'$$

Scheme III

In scheme III R_2 and $AR'R$ correspond to closed channel-receptor assemblies and A_2R_2', to an open assembly. Each receptor site binds acetylcholine equivalently and independently in the dimeric assembly, and thus schemes II and III are compatible and sufficient to define both acetylcholine binding and ion channel opening. An alternative formulation of scheme III in which agonist binding at the first (unoccupied) site in the dimeric assembly equilibrates rapidly relative to that at the second site (Sheridan and Lester, 1977) could be modeled by an extension of schemes II and III.

Acetylcholine Removal by Esterase

Numerous studies have demonstrated that a minimal mechanism for the hydrolysis of acetylcholine by acetylcholinesterase (E) is given by scheme IV (see Nachmansohn and Wilson, 1951; Rosenberry, 1975).

$$A + E \underset{k_{-1}^E}{\overset{k_1^E}{\rightleftharpoons}} AE \xrightarrow[\text{choline}]{k_2^E} acE \xrightarrow[H_2O]{k_3^E} E + \text{acetate} + H^+$$

$$acE + A \underset{k_{-i}}{\overset{k_i}{\rightleftharpoons}} A \cdot acE$$

Scheme IV

In scheme IV, the species AE is the Michaelis complex of acetylcholine and enzyme; acE is an acylated enzyme intermediate; and $A \cdot acE$ is a complex of acetylcholine and acE that is responsible for substrate inhibition of the enzyme. Although some controversy about the mechanism of substrate inhibition exists (Aldridge and Reiner, 1969), strong evidence indicates that this inhibition arises from the binding of acetylcholine to the active site in the acetylenzyme with consequent block of deacylation (Krupka and Laidler, 1961; Rosenberry and Bernhard, 1972) as shown in scheme IV.

Reduction of scheme IV can be accomplished by assuming that reversibly linked species rapidly achieve relative steady states compared with the time-course of epcs. In other words, $[AE]$ achieves a steady state with $[A]$ and $[E]$ so that $[A] + [AE] = [A](1 + [E]/K_m)$ where $K_m = (k_{-1}^E + k_2^E)/k_1^E$. This assumption is well supported experimentally, because a minimal rate of attainment of this steady state is k_2^E which has been estimated to be about 10^5 s^{-1} (Wilson and Cabib, 1956; see Rosenberry, 1975). Likewise $[A \cdot acE]$ is equilibrated with $[acE]$ so that $[acE] + [A \cdot acE] = [acE](1 + [A]/K_i]$ where $K_i = k_{-i}/k_i$. No direct

experimental evidence supports this assumption; but K_i for the eel enzyme has a high value of 44 mM (Rosenberry and Bernhard, 1972), suggesting that k_{-i} is rather large and rapidly establishes this steady state.

Acetylcholine Removal by Diffusion

Diffusion is difficult to introduce in a simple quantitative treatment of epcs because of the spatial inhomogeneities inherent in the diffusion equation $d[A]/dt = Dd^2[A]/dx^2$, where t is time; D is the diffusion constant for acetylcholine; and x is a spatial coordinate for one-dimensional diffusion. Eccles and Jaeger (1958) have considered the loss of acetylcholine by linear diffusion from a long striplike synaptic cleft of transverse dimension l (Fig. 2) that is devoid of secondary folds according to Eq. 1:

$$\frac{A}{A^0} \simeq \frac{8}{\pi^2} e^{-k_D t}. \tag{1}$$

In Eq. 1, A is the total amount of acetylcholine remaining in the cleft; and $k_D = \pi^2 D/l^2$. The qualitative effect of secondary junctional folds would be to increase the effective l value, but such an effect is ignored in this analysis. Additional terms in the series solution for A (Eccles and Jaeger, 1958) are small and have been neglected. Eq. 1 was derived by Eccles and Jaeger for diffusion in the absence of chemical reaction but was assumed to apply to the case of simultaneous diffusion and reaction. Eq. 1 suggests that diffusion from the cleft may be modeled as a first order process according to scheme V. Although Eq. 1 and scheme V do

$$A \xrightarrow{k_D} A_{\text{outside}}$$

Scheme V

adequately consider the concentration gradient set up by diffusion in the determination of k_D, the kinetic rate equations in the following section consider A to be homogeneously distributed in the reaction space. This approximation appears relatively undamaging to the overall analysis, particularly when $[A^0]$ is small relative to $[R^0]$ and $[E^0]$.

In the two-reaction space model (Fig. 2 *b*), acetylcholine diffusion from the first to the second reaction space is approximated as radial diffusion from the cylindrical surface of a flattened circular disk. Diffusion between the flattened ends of the disk is assumed to be sufficiently rapid ($\simeq$1 μs, Steinbach and Stevens, 1976) that concentration inhomogeneities parallel to the cylindrical axis can be ignored. Diffusion from the first to the second reaction space may be modeled by scheme VI, where A_I is the total amount of acetylcholine in the first reaction space and A_{II}, that in the second. However, in contrast to scheme V, where $[A]_{\text{outside}}$

$$A_I \xrightarrow{k_{D_I}} A_{II}$$

Scheme VI

at the cleft boundary is effectively zero and thus permits the application of Eq. 1, $[A]_{II}$ at the reaction space boundary is significant. As a consequence, k_{D_I} is not a first order rate constant like k_D but is a time-dependent parameter defined by the following derivation. If A_I is initially released from a line source corresponding to the cylindrical axis of the first reaction space, then A_I is given by Eq. 2,

$$A_1 = A^0(1 - e^{-1/k_0 t}), \tag{2}$$

where A^0 is the total initial quantity of acetylcholine; $k_0 = 4D/a^2$; and a is the radius of the flattened circular disk that corresponds to the first reaction space (Crank, 1957). Eq. 2 assumes radial diffusion in the absence both of chemical reaction and of acetylcholine loss from the synaptic cleft. Then the corresponding rate equation is given by Eq. 3:[2]

$$\frac{dA_1}{dt} = \frac{A^0 e^{-1/k_0 t}}{k_0 t^2} \simeq \frac{k_0 (A_1)^2}{A^0}. \tag{3}$$

According to Eq. 3, k_{D_1} in scheme VI is approximated by $k_0 A_1/A^0$; at $t = 0$, $k_{D_1} = k_0$. Although derived for initial release from a line source, this approximation of k_{D_1} appears to hold for an even greater time range if A_1 is initially distributed homogeneously in the first reaction space,[2] as postulated here in the two-reaction space model.[3]

This derivation of the diffusion rate coefficient of k_{D_1} can be extended to apply to the case of simultaneous diffusion and chemical reaction simply by replacing A^0 with $A_T = A_I + A_{II}$ as shown in Eq. 4:

$$k_{D_1} \simeq k_0 A_1/A_T \tag{4}$$

Eq. 4 models the time dependence of k_{D_1} in an accurate manner that is readily applied to analog computer circuitry.

RATE EQUATIONS

The rate equations that follow from schemes II, III, IV, and V are given in Eqs. 5–8.

$$\frac{d[AR']}{dt} = k_R[R][A] - k_{-R}[AR'] \tag{5}$$

$$\left(1 + \frac{[E]}{K_m}\right)\frac{d[A]}{dt} \simeq \frac{d([A] + [AE])}{dt} = -(k_R[R] + k_E[E] + k_D)[A] + k_{-R}[AR'] \tag{6}$$

$$\frac{d[A_2R_2]}{dt} = k_R[A][AR'R] - 2k_{-R}[A_2R_2'] \tag{7}$$

---

[2]The approximate equality on the right side of Eq. 3 is demonstrated by substitution of Eq. 2 into Eq. 3 followed by use of the approximation $x^2e^{-x} \simeq (1 - e^{-x})^2$ where $x = 1/k_0 t$. This approximation is valid here for $x \leq 2$; for $x = 2$, the error is 38%; for $x \leq 1$, the error is $\leq 8\%$. For a typical k_0 value of $10^4\ s^{-1}$, $x \leq 2$ when $t \geq 50\ \mu s$, virtually the entire time-course of an epc. Differential equations in the two-reaction space model assume that A_1 is initially distributed homogeneously over the first reaction space. The resultant expression for A_t corresponding to Eq. 2 is quite complex (cf. Eqs. 3.10b, c in Crank, 1957), but it appears that dA_1/dt in this case can be represented by the right-hand expression in Eq. 3 to within a factor of two for $2 \leq x \leq 100$ in addition to meeting the error limits in the previous sentences.

[3]The approximation of radial diffusion from a cylindrical disk is less valid when the first reaction space element sits directly over a secondary fold (as one element is shown in Fig. 2 *b*). Such a situation, however, should increase the effective k_{D_1} in scheme VI by at most 50% and have an even smaller effect upon the amplitudes of the simulated epcs. For example, when this situation involves the extensive secondary folds in frog muscle, the geometry of the first space element could be modified to include an additional half cylindrical disk of equivalent radius and height fused to the original so that its cylindrical axis intersects the original axis at right angles. For a fixed first space element volume, the modified element then would have about 20% smaller radii than the original disk and would correspond to an $\simeq$ 50% higher k_0 value.

$$\left(1 + \frac{[A]}{K_i}\right)\frac{d[acE]}{dt} \simeq \frac{d([acE] + [A \cdot acE])}{dt} = k_E[E][A] - k_3^E[acE]. \quad (8)$$

Eqs. 6 and 8 invoke the steady-state assumptions following scheme IV and define $k_E \equiv k_2^E/K_m$ (k_E is identical to the term k_{cat}/K_{app} in Rosenberry, 1975). These four equations are the basis of the epc simulations that follow. Note that the only contributions of esterase to the time-course of acetylcholine binding to receptor are the terms involving $[E]$ in Eq. 6. Whenever the approximation $[E] \simeq [E^0]$ is applicable, Eq. 8 is irrelevant to $[E]$ and hence to the epc simulations. This approximation is, of course, valid when $[E^0] \gg [A^0]$. However, it is also true at sufficiently low $[A]$ regardless of $[E^0]$; if $[A] \ll K_{app}$, where $K_{app} = K_m k_3^E/(k_2^E + k_3^E)$, $[E]$ is the only significant enzyme species. The observed value of K_{app} is 0.1 mM (Rosenberry, 1975), a value considerably above, for example, the initial maximum $[A] \simeq 1.5 \times 10^{-5}$ M arising from the homogeneous reaction space assumption.

RESULTS

A summary of the values of kinetic parameters to be used here for the solution of Eqs. 5–8 is given in Tables I and II. Several of these estimates were noted in the Introduction; in addition, k_E and k_3^E (see Rosenberry, 1975) and D (Peper et al., 1975; Eccles and Jaeger, 1958) are well established to the accuracy of the simulations. The estimate of k_{-R} comes from voltage-jump perturbations of clamped endplates (Sheridan and Lester, 1977) and from observed epc decay rates themselves (see Introduction). The overall acetylcholine dissociation rate constant from open channel receptor assemblies ($2k_{-R}$ in scheme III) appears rate limiting for epc decay when esterase is fully active (see Steinbach and Stevens, 1976), and the simulations here support this conclusion. The k_{-R} estimate in Table I agrees reasonably with a 1.4×10^2 s^{-1} dissociation rate constant measured by temperature-jump relaxation kinetics with isolated torpedo receptor (Neumann and Chang, 1976), especially when it is noted that the value of this overall rate constant appears voltage dependent in electrophysiological studies and thus may be poorly estimated by measurements on solubilized receptor. The transverse width l is taken to be 4 μm (frog neuromuscular junction; Eccles and Jaeger, 1958).

SIMULATION ASSUMING A HOMOGENEOUS REACTION SPACE

Within the context of the homogeneous reaction space model in Fig. 2 *a*, solutions to Eqs. 5–8 can be written directly (see Appendix I). Normalized concentration profiles for $[A]$, $[AR']$, and $[A_2R_2']$ corresponding to Eqs. 9A–11A were generated with an analog computer and are shown in Fig. 3 *a–c*. Free acetylcholine, A/A^0, decays very rapidly (Fig. 3 *a*), whereas

TABLE I
SUMMARY OF CONSTANTS USED IN THE KINETIC ANALYSIS

Symbol	Description	Total quantity per endplate
R^0	Total receptor	2×10^7 sites
E^0	Total esterase	2×10^7 sites
A^0	Total acetylcholine per epc	4×10^6 molecules
V	Endplate volume	450 μm^3
l	Transverse width of endplate	4 μm

TABLE II
SUMMARY OF RATE CONSTANTS USED IN THE KINETIC ANALYSIS*

Symbol	Value
k_R	$2 \times 10^7\ M^{-1}\ s^{-1}$
k_{-R}	$5 \times 10^2\ s^{-1}$
k_E	$2 \times 10^8\ M^{-1}\ s^{-1}$
k_3^E	$1.5 \times 10^4\ s^{-1}$
D	$1 \times 10^{-5}\ cm^2/s$

*25°C, 0.1 M ionic strength.

receptor-bound acetylcholine, AR'/A^0, shows growth and decay phases (Fig. 3 *b*). The calculated time t_p to peak binding of acetylcholine is 0.22 ms, and the calculated maximum value of AR'/A^0 is $AR'_{max}/A^0 = 0.079$. If occupied sites AR' were equivalent to open ion channels, these values would be in reasonable agreement with electrophysiological estimates noted in the Introduction. However, experimental evidence cited above suggests a dimeric receptor-channel assembly; and calulated profiles in the presence of esterase inhibitors fail to correspond to electrophysiological observations, as noted in the following paragraph. Thus this

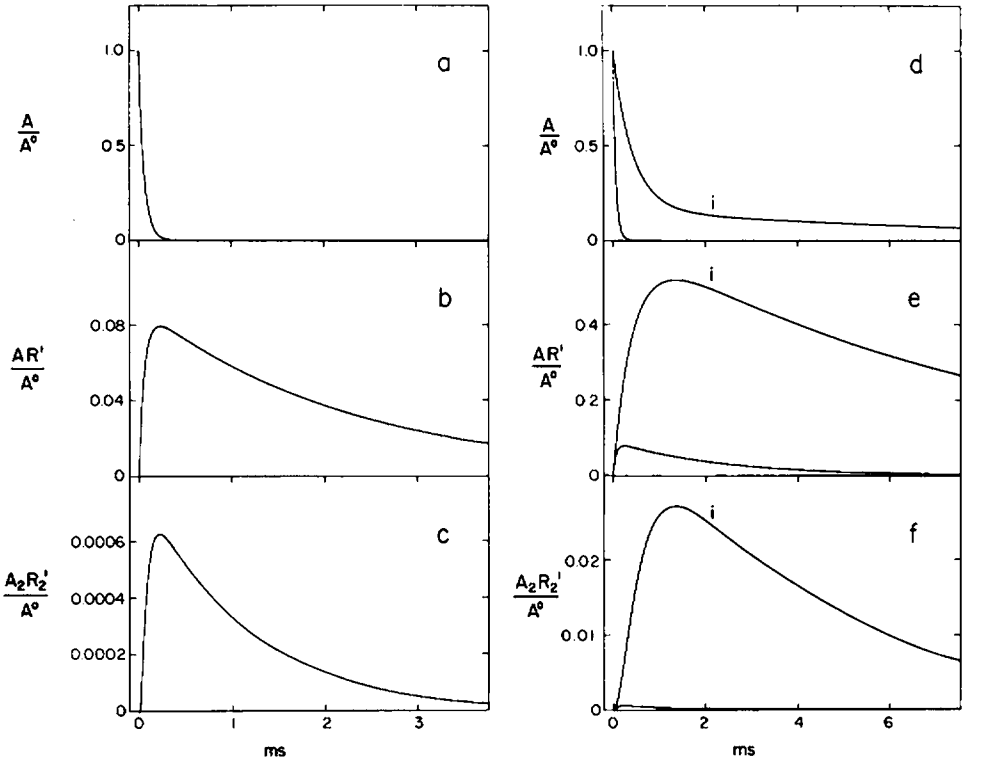

FIGURE 3 Concentration profiles that arise from simulations based on the homogeneous reaction space model (Eqs. 9A–11A). Symbols for the chemical species and rate equations that define the simulations are given in the text. (*a–c*) Esterase fully active; (*d–f*) esterase either fully active or completely inhibited (curves denoted by i). Note change in time scale in *d–f*.

initial agreement appears largely coincidental. The concentration of open ion channels $[A_2R'_2]$ also is biphasic (Fig. 3 *c*) with the same t_p as that for (AR'). However, $A_2R'_{2max}/A^0 = 0.00063$. This very small value is not supported experimentally and arises from the low probability of simultaneously occupying both sites of a dimeric receptor-channel assembly when $[R^0] = 5[A^0]$, as indicated for the homogeneous reaction space model here (see Table I). The start of the growth phase is sigmoidal; and the reciprocal time constant for the decay phase is $2\tau_\beta^{-1} = 8.9 \times 10^2\ s^{-1}$, twice the reciprocal time constant for the decay phase of $[AR']$. The value of τ_β^{-1} is only slightly less than the dissociation rate constant k_{-R}. The agreement of $2\tau_\beta$ with electrophysiological estimates of the decay phase time constant is of course dictated by the input value of k_{-R} as noted above.

Growth times and, to a large extent, maximum concentrations in Fig. 3 *b* and *c* are under the dominating influence of the esterase bimolecular reaction flux $k_E[E^0]$ (see Tables I and II and Eq. 4A). Thus, within this homogeneous reaction space assumption, growth times, t_p values, and maximum concentrations are very sensitive to esterase inhibition as shown in Fig. 3 *d–f*. When complete esterase inhibition is assumed ($[E^0] = 0$), free acetylcholine $[A]$ decays more slowly (Fig. 3 *d*). Peak binding of acetylcholine now occurs at 1.30 ms, and AR'_{max}/A^0 increases 6.5-fold to 0.52 (Fig. 3 *e*). Even more striking is the 43-fold increase in $A_2R'_{2max}/A^0$ resulting from esterase inhibition (Fig. 3 *f*). Such dramatic effects arising from esterase inhibition are not observed on experimentally measured mepcs and epcs, as noted in the Introduction. Despite the fact that the traces in Fig. 3 *d–f* can be altered somewhat by assuming some variation in $[R^0]/[E^0]$ ratios, these discrepancies between predicted epcs and experimentally observed epcs and mepcs lead to the conclusion that the homogeneous reaction space assumption is inappropriate for the growth phase of epcs and mepcs. An alternative model is considered in the next section.

Even though Eq. 11A arising from the homogeneous reaction space model appears invalid for the simulation of the entire time-course of epcs, it accounts quite well for the decay phase. The decay phase reciprocal time constant $2\tau_\beta^{-1}$ decreases 3.8-fold to $2.3 \times 10^2\ s^{-1}$ on complete esterase inhibition in Fig. 3 *f*. This is in reasonable agreement with the electrophysiological estimates in the Introduction. The magnitude of this calculated decrease is very sensitive to the assumed value of k_D (Eq. 1) and hence to the cleft transverse dimension l (Table I). If mammalian endplates are characterized by a somewhat larger value of l than the 4 μm used here (see Salpeter and Eldefrawi, 1973), a somewhat greater decrease may be expected (see Rang, 1975). Conversely, if l is smaller in many frog endplates (Steinbach and Stevens, 1976), a smaller decrease would obtain.

It is noteworthy that τ_β^{-1} in the absence of esterase is not simply the diffusion rate k_D but instead is given by Eq. 9, where $K_R = k_{-R}/k_R$:

$$\tau_{\beta([E^0]=0)}^{-1} \cong \frac{k_D}{1 + \dfrac{[R^0]}{K_R} + \dfrac{k_D}{k_{-R}}}. \tag{9}$$

Thus diffusion from the cleft is predicted in this simulation to be reduced by acetylcholine binding to receptor sites as originally proposed by Katz and Miledi (1973). The factor $(1 + [R^0]/K_R + k_D/k_{-R})$ by which diffusion is slowed includes not only the equilibrium binding term $[R^0]/K_R$ considered previously (Katz and Miledi, 1973; Magleby and Terrar, 1975; see

Colquhoun, 1975) but also the term k_D/k_{-R} which becomes very small if equilibrium is actually attained. In this analysis $[R^0]/K_R = 3$ but $k_D/k_{-R} = 1.2$; thus during the decay phase, acetylcholine is not equilibrated with receptor and diffusion is slowed by a net factor of 5.2. Blocking most receptor binding sites for acetylcholine with, for example, an α-neurotoxin is observed to restore the epc decay time constant to near its value in the absence of inhibitors (Katz and Miledi, 1973; Magleby and Terrar, 1975). This effect is also predicted by Eq. 9: for the remaining receptors now $\tau_\beta^{-1} \simeq k_D/(1 + k_D/k_{-R}) = k_D/2.2$; and the reciprocal time constant for epc decay becomes $2\tau_\beta^{-1} = 5.5 \times 10^2\ s^{-1}$, about 62% of its original value in the absence of inhibitors.

The agreement of predicted and observed decay phase time constants supports the use of the homogeneous reaction space assumption in the analysis of the epc decay phase. This assumption has also been used in previous analyses of the decay phase (Eccles and Jaeger, 1958; Magleby and Stevens, 1972*a*; Kordas, 1972*a*). The decay phase reciprocal time constant $2\tau_\beta^{-1}$, approximated by $2k_{-R}$ in the absence of inhibitors, still retains (*a*) a direct dependence on k_{-R} after esterase inhibition and (*b*) even a partial dependence after the blocking of all esterase and of most receptor sites (see Eqs. 8A and 9). Thus $2\tau_\beta^{-1}$ is predicted to retain virtually the total voltage dependence of k_{-R} under the first condition and some voltage dependence under the second. This first prediction is experimentally supported, and the second prediction appears supported by less direct evidence (Magleby and Stevens, 1972*b*).

SIMULATION ASSUMING TWO-REACTION SPACES

Because endplate current simulations based on a homogeneous reaction space fail to represent adequately the entire time-course of the epcs, alternative simulation models can be considered. The most obvious weakness of the homogeneous reaction space model is its incorrect prediction of large increases in epc growth times and amplitudes after esterase inhibition. This weakness arises from the relative overall bimolecular reaction rates of acetylcholine with receptor and esterase given in Table II; the receptor rate constant k_R is about an order of magnitude smaller than the esterase rate constant k_E. Thus active esterase effectively removes most acetylcholine before it can react with receptor. This weakness is overcome if the acetylcholine reactions are postulated to occur in two-reaction spaces or two-reaction compartments (Fig. 2 *b*). The first reaction space (I) initially contains all the released acetylcholine. This acetylcholine is distributed homogeneously at a relatively high concentration (stoichiometrically in excess of the total receptor and esterase sites) so that esterase sites are transiently saturated and receptor sites become sufficiently occupied. The second reaction space (II) is simply the remainder of the synaptic cleft and receives acetylcholine by diffusion from the first reaction space.

Most kinetic constants will retain the values in the two-reaction space model that they held in the homogeneous reaction space model. However, two major complications to the homogeneous reaction space model are involved in extending it to a two-reaction space model. The first complication is operational: Eqs. 5–8 now obtain in the first reaction space, and these are not linear differential equations because the bimolecular reaction rates are all second order. Thus simulation can be conducted only on a computer. In this report an analog computer is used, and the relevant transformations of Eqs. 5–8 and the analog computer

circuitry are shown in Appendix II. The second complication involves choices of the relative volumes, V_I and V_{II}, of the two-reaction spaces and the extent to which they are discrete or continuous. These choices determine the initial acetylcholine concentration in the first reaction space, $[A^0]_I$; the total number of receptors in the first reaction space, R_I^0; and the diffusion rate coefficient, k_{D_I}, for acetylcholine diffusion from the first reaction space to the second (the subscripts I, II, or T will designate a species in the first, the second, or the total of both reaction spaces, respectively).

Before epc simulations in the two-reaction space model are illustrated, appropriate alterations of values of kinetic terms from those used in the homogeneous reaction space model will be identified. No changes will be made in the second reaction space, except that the initial acetylcholine concentration $[A^0]_{II}$ is zero and that acetylcholine appears only by diffusion from the first reaction space. Acetylcholine diffuses from the second reaction space into the cleft as modeled above in the homogeneous reaction space model. The second reaction space remains well represented by Eq. 1A, but Eq. 2A must be replaced by Eq. 10.

$$\frac{d[A]_{II}}{dt} = k_{D_I}[A]_I - (k_R[R^0]_{II} + k_E[E^0]_{II} + k_D)[A]_{II} + k_{-R}[AR']_{II}. \quad (10)$$

Inclusion of additional terms corresponding to second order bimolecular reaction rates (cf. Eqs. 13A–15A with Eqs. 17A–19A) alters concentration simulations in the second reaction space by <5% and can be ignored. In the first reaction space a fivefold higher total receptor concentration $[R^0]_I$ will be assumed. This change is required because receptor densities per unit area of postsynaptic membrane are about threefold higher in juxtaneuronal regions than in calculated averages which assume R_T^0 to be evenly distributed over the entire postsynaptic membrane (Fertuck and Salpeter, 1976) and because the first reaction space is assumed to be a juxtaneuronal disk 50 nm thick (see Fig. 2 *a*). Eqs. 5–8 obtain for the first reaction space with k_{D_I} replacing k_D, and it is again assumed that $[AE] \simeq 0$. Mass conservation equations $[R]_I = [R^0]_I - [AR']_I$; $[ARR']_I = [AR']_I - 2[A_2R_2']_I$; and $[E]_I = [E^0]_I - (1 + [A]_I/K_i)[acE]_I$ permit elimination of $[R]_I$, $[ARR']_I$, and $[E]_I$ from these equations.

The two-reaction space model is constructed in the following manner. Consider a juxtaneuronal first reaction space with $[R^0]_I = 5[R^0]_{II} = 3.75 \times 10^{-4}$ M. For the initial $[A^0]_I$ to exceed $[R^0]_I + [E^0]_I$, the rather arbitrary assumption that $[A^0]_I = 2[R^0]_I$ is made, although this choice is less critical than may at first appear (see below). The last remaining parameter necessary for epc simulation is the diffusion coefficient k_{D_I} given by Eq. 4. Estimation of the constant k_0 in this coefficient requires assumptions about the volume and geometry of the first reaction space (Eq. 2 ff.). Some of these assumptions have been noted earlier, but the full development is as follows. The assumed value of $[A^0]_I = 7.5 \times 10^{-4}$ M is 50-fold higher than that of $[A^0]$ in the earlier homogeneous reaction space model; and, as the total amount of acetylcholine is the same in either model, the first reaction space volume, V_I, must correspond to 1/50 of the total junctional cleft volume, $V_I + V_{II}$. Furthermore, the first reaction space is assumed to be a collection of discrete elements rather than a continuous reaction space (Fig. 2 *b*). To determine the number of such elements involved in an epc, it is assumed that an mepc corresponds to a miniature conductance involving a single element and that, during an epc, the conductance from all elements sum linearly. Thus the number of elements n = (peak conductance epc)/(peak conductance mepc) $\simeq$ 10,000 nmho/65 nmho

$\simeq$ 150 for both rat diaphragm and frog muscle endplates (Colquhoun, 1975). The term n approximates a minimum estimate of the quantal content in the neurotransmitter theory because it ignores nonlinear summation. The reaction volume of each element n then is $1/50 \times 1/150 \times 450\ \mu m^3 = 0.06\ \mu m^3$. This volume corresponds to a disk element with a height of 0.05 μm and radius a of 0.62 μm (Fig. 2 *b*). The resulting estimate of $k_0 = 4D/a^2$ is $1.0 \times 10^4\ s^{-1}$.

Inspection of Component Profiles

Four independent species variables, A, AR', A_2R_2', and acE, are sufficient to define epc simulations in the two-reaction space model. A fifth species variable, the substrate-inhibited esterase form, $A \cdot acE$, will be shown below to be negligible. The time-course of each species in either reaction space is determined by the analog computer solutions. Because two reaction spaces are being considered, each species will be described in relative moles (rather than concentration) normalized to the initial total moles of acetylcholine A_T^0 (in addition to subscripts I, II, or T, a second subscript i will denote a species in the presence of complete esterase inhibition).

Before examining in detail the component profiles in Fig. 4, one may note that the discrepancies between predicted and experimentally observed epcs and mepcs which forced extension of the homogeneous reaction space model have disappeared in the two-reaction space model. Dimeric receptor-channel assemblies A_2R_2' in Fig. 4 *d* that are assumed

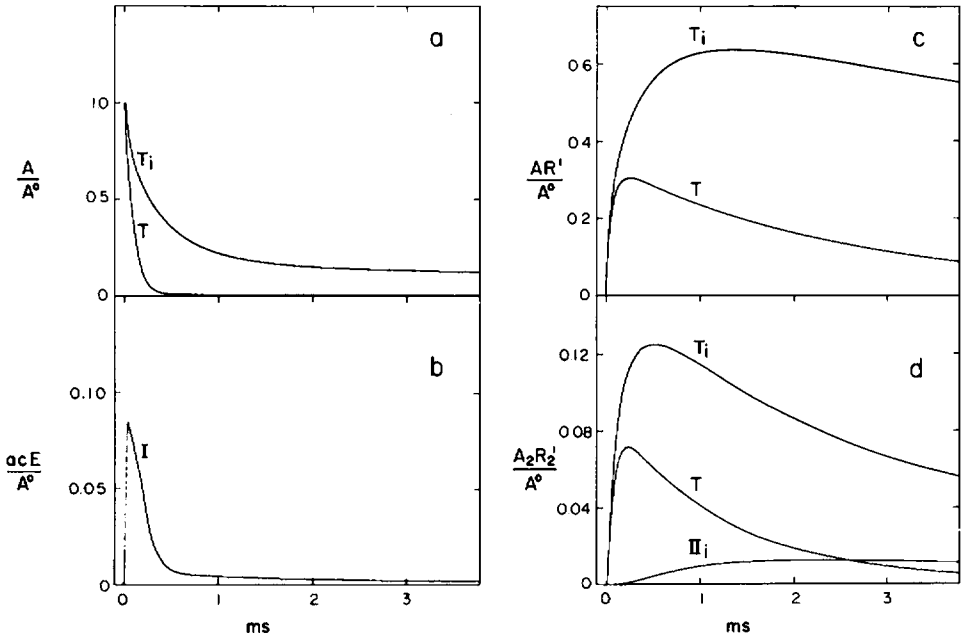

FIGURE 4 Component profiles that arise from simulations based on the two-reaction space model. Chemical species are indicated by the same symbols used in Fig. 3, and the simulations were conducted as outlined in the text and illustrated in Appendix II (Table IV). The designations I, II, or T refer to the normalized amount of a species in the first, the second, or the total of both reaction spaces, respectively; the subscript i further indicates a simulation in which esterase is completely inhibited.

proportional to the epc give $A_2R'_{2_{T(max)}}/A^0_T = 0.071$ and $A_2R'_{2_{T(max)}}/A^0_T = 0.123$. Furthermore, the growth time defined according to Gage and McBurney (1975) for $A_2R'_{2_T}$ increases from 70 μs initially to 140 μs after esterase inhibition (corresponding t_p values are 220 and 400 μs, respectively). Therefore, the following simulated values are in reasonable agreement with the electrophysiological estimates noted in the Introduction: the relative maximum number of open channels, 7.1% of the total released acetylcholine in the uninhibited endplate; the 1.7-fold increase in epc amplitude after esterase inhibition; and the absolute values of the growth times under both conditions.

Four features of the two-reaction space model contribute to this improvement from the earlier homogeneous model. Consider three of these features first in the absence of esterase inhibition. One feature is the fivefold increase in total receptor concentration $[R^0]_I$ in the first reaction space. This feature alone largely accounts for the increase in acetylcholine-bound receptor AR'_T between Fig. 3 *b* and Fig. 4 *c*. To illustrate, the calculated AR'_{max}/A^0 for the homogeneous reaction space model at the higher $[R^0] = 3.75 \times 10^{-4}$ M is 0.30 (see Eq. 10A), the same as the simulated value in Fig. 4 *c*. This increase in $[R^0]$ alone would give rise to a threefold increase in $A_2R'_2/A^0$ in the homogeneous model (see Eq. 11A). A second feature of the model of greater importance to increasing the relative amount of $A_2R'_{2_T}$ is the increased concentration of A in the small volume of the first reaction space and the consequent partial saturation of receptor sites. Acetylcholine maximally occupies 53% of the total receptor sites in the first reaction space, and the corresponding high probability of forming $A_2R'_{2_I}$ accounts for virtually all the $A_2R'_{2_T}/A^0_T$ in Fig. 4 *d*. Although some 54% of the total acetylcholine does reach the second reaction space, <7% of it forms AR'_{II} and only 0.04% forms $A_2R'_{II}$. A third feature which also contributes to the increased concentration of A in the first reaction space is the partial saturation of the esterase in the form of acE. As shown in Fig. 4 *b*, acE_I has a much shorter lifetime than receptor-acetylcholine complexes due to its high deacetylation rate constant. Nevertheless, the even higher esterase acetylation rate results in maximal conversion of about 84% of E^0_I to acE_I. This partial saturation of the esterase slows acetylcholine hydrolysis and decreases the $[A]_I$ decay rate nearly 50%. Slower $[A]_I$ decay allows greater binding to receptor sites, and the net result is that $A_2R'_{2_T}$ is increased twofold over that in the hypothetical case where an infinite esterase deacetylation rate prevents saturation. Rapid depletion of A_I both by hydrolysis and by diffusion insure that k_{-R} remains essentially rate limiting during the epc decay phase. The decay phase is a single exponential in Fig. 4 *d*, and the reciprocal time constant is only 15% smaller than that for the homogeneous model in Fig. 3 *c*.

When esterase is inhibited, all acetylcholine eventually reaches the second reaction space according to the model. The resultant profiles of A_{T_i}/A^0_T and AR'_{T_i}/A^0_T in Fig. 4 *a* and *c* are very similar to those in Fig. 3 *d* and *e* for the homogeneous model. Now acetylcholine maximally occupies 69% of the total receptor sites in the first reaction space, and at t_p, $A_2R'_{2_{I_i}}$ is about 95% of $A_2R'_{2_{T_i}}$. However, acetylcholine diffusion to the second reaction space results in an accumulation of $A_2R'_{2_{II_i}}$ as shown in Fig. 4 *d*. The summation of $A_2R'_{2_{I_i}}$ in both reaction spaces underlies the fourth feature of the two-reaction space model. This feature is that, although $A_2R'_{2_{I_i}}$ determines both the amplitude and t_p for $A_2R'_{2_{T_i}}$, both $A_2R'_{2_{I_i}}$ and $A_2R'_{2_{II_i}}$ contribute to the decay phase. The decay phase for $A_2R'_{2_{T_i}}$ in Fig. 4 *d* in fact is not a single exponential but is slightly biphasic: from 0.7 to 3.0 ms the reciprocal time constant is 2.7 $\times$

$10^2\ s^{-1}$, and beyond 3.0 ms the reciprocal time constant drops some 20% below the value of $2.3 \times 10^2\ s^{-1}$ simulated in the esterase-inhibited homogeneous reaction space model. Such a slightly biphasic decay of epcs after esterase inhibition has not been noted in electrophysiological reports. Whereas the biphasic nature of this decay may be an artifact induced by the approximation inherent in limiting the synaptic cleft to two reaction spaces, it seems theoretically plausible. The term k_{D_1} substantially contributes to the rate of decay after esterase inhibition, and this term is not a constant according to Eq. 4. Thus the application of Eq. 9 to the decay phase should be tempered by the realization that the k_D in this equation is an approximate average value corresponding to diffusion both within and from the synaptic cleft.

Relative Reaction Volumes in the Two-Reaction Space Model

Component profiles in Fig. 4 *a–d* involve the assumption that $[A^0]_I = 2[R^0]_I$ or that V_I of the first reaction space corresponds to 2% of the total reaction space. The effect of increasing or of decreasing V_I relative to V_{II} by a factor of two is demonstrated in Fig. 5 *a–c*. A relatively small effect of these changes on the simulated epcs is observed for the reasons outlined in the following example. A twofold decrease in V_I forces a twofold decrease in the area of each reaction element disk in the first reaction space and thus a twofold decrease in the total amount of receptor R_I^0 in the first reaction space. Consequently, the diffusion rate coefficient k_{D_1} from the first to the second reaction spaces is increased twofold (see Eqs. 3 and 4). The effects of the higher $[A^0]_I$, lower R_I^0, and the higher k_{D_1} tend to cancel. The ratio $A_2R'_{2_T}/A_T^0$ remains virtually unchanged in Fig. 5 *a* and *b* and decreases only 25% in Fig. 5 *c*. After esterase inhibition, the value of R_I^0 is somewhat more dominant than the other two effects, but the total variation in $A_2R'_{2_{T_1}}/A_I^0$ in Fig. 5 *a–c* is still less than about 50% at any time point. Changes in V_I/V_T by more than a factor of two tend to collapse the analysis to that of the homogeneous reaction space model: at low V_I/V_T, the small value of R_I^0 renders the first reaction space inconsequential; whereas at high V_I/V_T, the first and second reaction spaces merge into a homogeneous space. The initial condition $[A^0]_I = 2[R^0]_I$ appears both to average alternative two-reaction space conditions reasonably well and to optimize the adequacy of a two-reaction space model to represent more precise multireaction space models.

Substrate Inhibition of Esterase Activity by Acetylcholine is Negligible

Analog computer circuitry which includes substrate inhibition arising from the binding of acetylcholine to acetylated esterase (scheme IV) is included in Fig. 7 in the Appendix. Such inhibition contributes $<10\%$ to the amplitude of simulated epcs even when the simulated K_i for A binding to acE is set equal to A_I^0 (Fig. 6). However, experimental data suggest that the actual K_i value (4×10^{-2} M noted earlier) is much higher than the $[A^0]_I = 7.5 \times 10^{-4}$ M in Fig. 6. Consequently, esterase inhibition by substrate can be expected to contribute $<1\%$ to the amplitude of epcs.

DISCUSSION

The successful epc simulations obtained with the two-reaction space model here permit two major conclusions about acetylcholine action at neuromuscular junctions. First, the time-

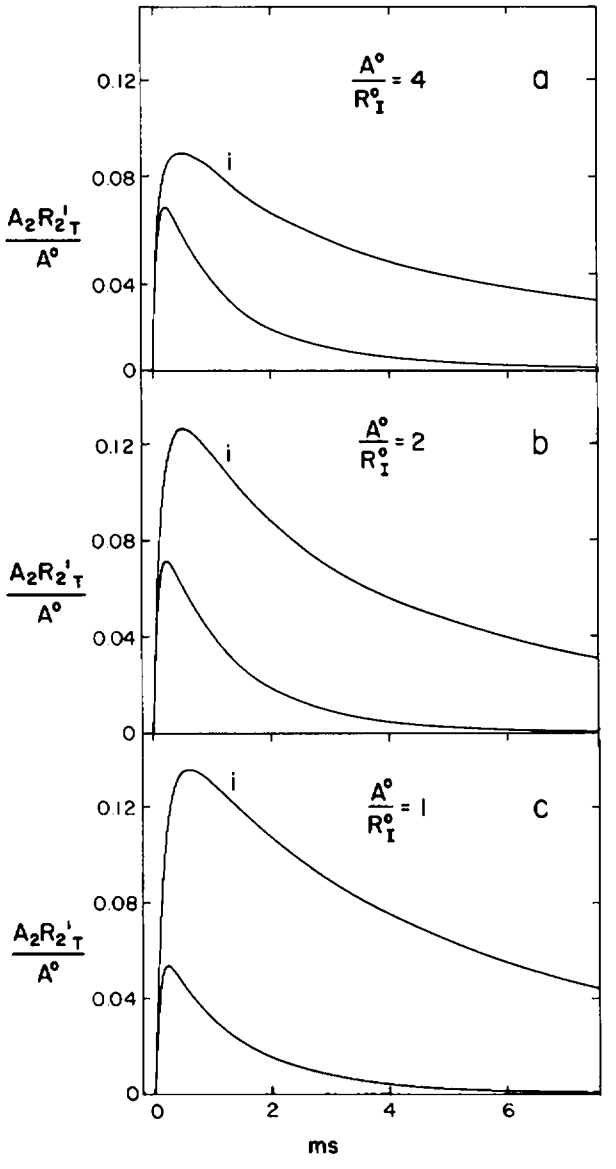

FIGURE 5 Relative volumes of the first reaction space and its effect on epc simulations in the two-reaction space model. The time dependence of the relative number of open ion channels is shown both with fully active and with completely inhibited (i) esterase. In each figure, the ratio of the initial number of acetylcholine molecules to the total number of receptor sites in the first reaction space is indicated. These ratios arise from the relative volumes of V_1 and V_T: (*a*) $V_1/V_T = 0.01$; (*b*) $V_1/V_T = 0.02$; (*c*) $V_1/V_T = 0.04$. The relative reaction volume, V_1/V_T, directly enters the analog computer simulations as a scaling factor (see Tables III and IV in Appendix II).

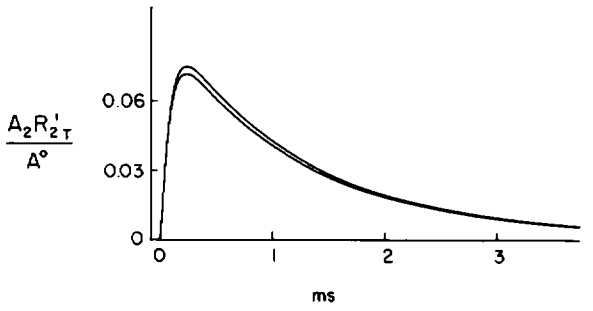

FIGURE 6 The effect of esterase inhibition by acetylcholine on epc simulations in the two-reaction space model. Esterase inhibition is modeled according to scheme IV and applied to the epc simulation in Fig. 4*d* in which esterase is otherwise fully active. Detailed simulation conditions are given in Fig. 7 and Table IV in Appendix II. The upper trace corresponds to substrate-inhibited esterase ($p_6 = 1.0\ \text{volt}^{-1}$ in Table IV); and the lower trace, to fully active esterase in which substrate inhibition is neglected ($p_6 = 0$).

course and amplitudes of epcs are primarily determined by the chemical reaction rates that characterize acetylcholine interactions with receptor and esterase. These reaction rates are not instantaneous relative to diffusion, and thus the interactions occur under nonequilibrium conditions in which the rate of acetylcholine diffusion within the synaptic cleft progressively alters the reaction rates. Second, the cooperative opening of ion channels by acetylcholine requires that acetylcholine be introduced into the synaptic reaction space in discrete, concentrated elements for a sufficient number of channels to be opened during an epc. These general conclusions can be drawn regardless of the mechanism that underlies the cooperativity and would not be challenged by two- or threefold improvements in the estimates of the constants in Tables I and II that are used here. The concept of initial reaction space elements in which acetylcholine is concentrated is readily accommodated to proposals that concentrated acetylcholine is released from presynaptic vesicles (Katz, 1969) to interact with postsynaptic membrane compartments that are structurally and functionally discrete (see Steinbach and Stevens, 1976; Hartzell et al., 1975).

Both the homogeneous and the two-reaction space models developed here extend previous quantitative treatments of epcs (Kordas, 1972*a*; Magleby and Stevens, 1972*b*) by introducing sufficient sets of differential equations which are then solved with the use of experimentally measured reaction rate constants. The accuracy of these solutions is limited by several assumptions, most of which were introduced and defended earlier. The following summary notes the more important of these assumptions: (*a*) Rate constant values taken largely from electric organ receptor and esterase preparations are applicable to these proteins in neuromuscular junctions; (*b*) a single class of receptor sites and a single class of esterase sites define the only acetylcholine interactions in the synapse; (*c*) cooperativity arises from a requirement of two acetylcholine-bound receptor sites per open ion channel; (*d*) diffusion of acetylcholine both within and from the synaptic cleft can be based on simple geometric models; and (*e*) the endplate conductance increase during epcs is a linear summation of mepc conductance increases. A sixth assumption, that acetylcholine release is instantaneous relative to the time-course of epcs, is probably quite good for mepc simulations but less so for epc simulations. If an asynchronous release of acetylcholine into discrete elements occurs during

epcs (Katz and Miledi, 1965), the predicted epc growth times would be too short; but predicted epc amplitudes and decay times would be quite accurate. These assumptions are summarized by schemes II–VI and the corresponding differential Eqs. 5–8. The significant advantage obtained by simplifying the kinetic models to this extent is that the kinetic constant values required for epc simulations are limited to those in Table I. Of these quantities, the values of R^0, E^0, A^0, V, l, k_E, k_3^E, and D can be estimated quite directly and appear to be accurate within a factor of two according to the source references. The remaining constants, k_R and k_{-R}, are defined by the single overall receptor-acetylcholine interaction in scheme II, and some skepticism concerning the adequacy of this scheme is warranted. It must be emphasized that the overall k_R and k_{-R} rate constants are composites that incorporate intrinsic rate constants for binding and conformation change, just as k_E is an overall rate constant. Values of k_R and k_{-R} thus are obtained in a straightforward manner by voltage-jump perturbations of clamped endplates provided that single relaxations corresponding to a bimolecular reaction are observed, as in the data of Sheridan and Lester (1977). These estimates of k_R and k_{-R} are close to a factor of two agreement with less direct biochemical estimates of these constants, as noted above. Even if scheme II is only approximately correct, differential Eqs. 5–8 probably provide a satisfactory description of the system. It is reassuring that the two-reaction space simulation is in reasonable agreement with experimentally observed mepcs in five critical characteristics: the absolute rise time and the absolute amplitude, both in the presence and the absence of esterase; and the decay time in the absence of esterase relative to that in the presence of esterase. The component profiles in Fig. 5 *a–c* provide a general indication of the sensitivity of the simulations to variations in the input kinetic constants. Assumption five above corresponds to a quantal content estimate of 150, somewhat smaller than other estimates (see Kuffler and Yoshikami, 1975). A larger quantal content or a smaller number of acetylcholine molecules per quantum would result in smaller first reaction space element volumes, larger values of k_{D_1}, and consequent smaller amplitudes than those predicted in Fig. 5.

Several conclusions drawn in previous reports are supported by the simulations presented here. The lifetime of acetylcholine in the synaptic cleft is much shorter than epc decay times when esterase is fully active (Magleby and Stevens, 1972*b*). Initial acetylcholine concentrations in the first reaction space are sufficiently high to nearly saturate esterase sites (Fertuck and Salpeter, 1976) in the acetylenzyme form, although the simulations indicate that substrate inhibition of esterase is negligible. A high percentage of receptor sites in the first reaction space elements also are occupied by acetylcholine at the maximum epc (Negrete et al., 1972; Lester et al., 1978; Matthews-Bellinger and Salpeter, 1978); however, our simulations do not support the contention of these authors that receptor sites are saturated. Even though initial acetylcholine concentrations in the first reaction space are sufficiently high for equilibrated receptor sites to be saturated, equilibrium between receptor and acetylcholine is not achieved within the short time interval of these high concentrations. Of the total ion channels in the first reaction space, the simulations in Figs. 5 *a–c* predict that 68, 48, and 26%, respectively, are opened at the peak epc amplitude when esterase is inhibited. These percentages are in excellent agreement with corresponding estimates of 50–75% obtained from the observed potentiation of peak epcs by acetylcholine iontophoresis (Hartzell et al., 1975).

From the perspective of chemical kinetics upon which these simulations are based, several teleological observations can be made. Hartzell et al. (1975) have noted that cooperativity in acetylcholine-induced ion channel opening both increases epc signal to noise (low acetylcholine concentrations result in negligible epcs) and sharpens the epc time-course (epc decay rates are increased). This sharpening effect is particularly illustrated by the epc simulations in the absence of esterase in Fig. 4 *c* and *d*. The simulated epc decay (Fig. 4 *d*) not only occurs with a higher reciprocal time constant than that of the total acetylcholine-bound receptor sites (Fig. 4 *c*), but it also begins much earlier because open channels are virtually confined to the first reaction space, whereas acetylcholine-bound receptor sites are much more widely distributed. The correspondence of the simulated epc decay with the observed in this respect in fact provides additional supporting evidence that ion channel opening is cooperative. Esterase inhibition increases observed peak epc amplitudes about twofold. Thus esterase must be localized in the first as well as in the second reaction space where it both directly shapes the epcs by rapid acetylcholine removal and minimizes the loss of acetylcholine outside the synaptic cleft. Finally, this kinetic perspective suggests that one function of the postjunctional secondary folds is to trap the hydrolysis product choline and to minimize its diffusional loss outside the synaptic cleft. Choline in the cleft has been proposed to be taken into the nerve terminal by a high affinity choline uptake system, after which it is presumed to be acetylated and reused in synaptic transmission (see Dowdall et al., 1976). It is unlikely either that the number of high affinity choline uptake sites exceeds the number of receptor or esterase sites or that the uptake sites function more efficiently than esterase sites. Thus choline would tend to accumulate after acetylcholine release, and some trapping mechanism would appear essential to prevent its diffusional loss.

Although the epc simulations in this report are constructed for the neuromuscular junction, corresponding differential equations could in principle be formulated for other examples of synaptic transmission. Three rates are critical for such formulations: an overall rate of receptor activation which includes a transmitter-receptor association rate; a transmitter-receptor dissociation rate; and a transmitter removal rate that combines diffusional, degradative, and reuptake processes. Postsynaptic activation then arises from a dynamic competition between reversible receptor occupancy and irreversible transmitter removal.

APPENDIX I

Simulation Assuming a Homogeneous Reaction Space

Under this assumption $[R^0]$ amd $[E^0]$ are in excess of the total $[A^0]$ released during an epc, as noted in the Introduction. Then $[R] \simeq [R^0]$; $[E] \simeq [E^0]$; and Eq. 8 can be ignored. Eqs. 5 and 6 now determine the time-course of acetylcholine $[A]$ in the synaptic cleft as given in Eqs. 1A and 2A.

$$\frac{d[AR']}{dt} \simeq k_R[R^0][A] - k_{-R}[AR'] \tag{1A}$$

$$\left(1 + \frac{[E^0]}{K_m}\right)\frac{d[A]}{dt} \simeq -(k_R[R^0] + k_E[E^0] + k_D)[A] + k_{-R}[AR']. \tag{2A}$$

Values of kinetic terms in Eqs. 1A and 2A are readily determined from Tables I and II: $k_R[R^0] = 1.5 \times 10^3\ s^{-1}$; $k_E[E^0] = 1.5 \times 10^4\ s^{-1}$; and $k_D = 6 \times 10^2\ s^{-1}$ (see Eq. 1 ff.). A comparison of $k_E[E^0]$

with k_D leads to the prediction that about 96% of the released acetylcholine is removed by esterase hydrolysis and 4% by diffusion out of the cleft during an epc.

Eqs. 1A and 2A are simultaneous linear differential equations whose solutions can be written out in analytic form, as shown below. Eq. 7 also will be solved below with the use of the solutions to Eqs. 1A and 2A. Solutions to Eqs. 1A and 2A (Perrin, 1970) yield two reciprocal relaxation times τ_α^{-1} and τ_β^{-1} which are given by Eq. 3A, where τ_α^{-1} corresponds to the positive sign and τ_β^{-1}, to the negative sign.

$$\tau^{-1} = \frac{b}{2}\left[1 \pm \sqrt{1 - \frac{4c}{b^2}}\right] \tag{3A}$$

The constant terms b and c in Eq. 3A are expressions involving the individual rate constants in Eqs. 1A and 2A are defined in the following paragraph.

Although no further simplification is necessary for a precise mathematical description of the time dependence of $[AR']$ and $[A]$, two further approximations are suggested by the magnitudes of the individual rate constants which simplify the expressions. The first simplifying approximation is that the quantity $[E^0]/K_m \ll 1$ and hence is negligible compared with unity in Eq. 2A. This is equivalent to assuming a negligibly low steady-state $[AE]$. This assumption is justified by values of $K_{app} \cong 10^{-4}$ M, $k_2^E \cong 10^5\ s^{-1}$ and $k_3^E = 1.5 \times 10^4$ (pH 7.4; Rosenberry, 1975), from which one can estimate K_m to be about 6×10^{-4} M and $[E^0]/K_m$ to be about 0.1. With this assumption, b and c in Eq. 3A are given by Eqs. 4A and 5A.

$$b \cong k_R[R^0][A] + k_E[E^0] + k_D + k_{-R} \tag{4A}$$

$$c \cong (k_E[E^0] + kI)k_{-R}. \tag{5A}$$

The second simplifying approximation is that the quantity $4c/b^2 < 1$ so that τ^{-1} in Eq. 3A effectively includes only the first two terms of a power series as in Eq. 6A.

$$\tau^{-1} \cong \frac{b}{2}\left[1 \pm \left(1 - \frac{2c}{b^2}\right)\right] \tag{6A}$$

This assumption is justified by noting the values of $b \cong 2 \times 10^4\ s^{-1}$ and $c \cong 8 \times 10^6\ s^{-2}$. The reciprocal time constants τ_α^{-1} and τ_β^{-1} are now given by Eqs. 7A and 8A.

$$\tau_\alpha^{-1} \cong b - \frac{c}{b} \cong b \tag{7A}$$

$$\tau_\beta^{-1} \cong \frac{c}{b} \tag{8A}$$

Completing the matrix method, solution with the boundary condition that at time zero, $[A] = [A^0]$, one obtains the solutions for $[A]$ and $[AR']$ given in Eqs. 9A and 10A.

$$\frac{A}{A^0} = \frac{A}{\tau_\alpha^{-1} - \tau_\beta^{-1}}\left[(\tau_\alpha^{-1} - k_{-R})e^{-t/\tau_\alpha} + (k_{-R} - \tau_\beta^{-1})e^{-t/\tau_\beta}\right] \tag{9A}$$

$$\frac{AR'}{A^0} = \frac{k_R[R^0]}{\tau_\alpha^{-1} - \tau_\beta^{-1}}\left[e^{-t/\tau_\beta} - e^{-t/\tau_\alpha}\right]. \tag{10A}$$

In Eqs. 9A and 10A, $[A]$ and $[AR']$ are normalized by $[A^0]$; and hence the concentration brackets have been deleted. Eq. 7 for the dimeric receptor channel assembly is readily solved with the use of Eqs. 9A and 10A if it is assumed that $[AR'] \cong [AR'R]$. This approximation is reasonable within the homogeneous reaction space assumption: by definition $[AR'] \equiv [AR'R] + 2[A_2R_2']$, and because $[R^0] \gg [AR']$, then $[AR'R] \gg [A_2R_2']$. The corresponding solution to Eq. 7 is given in Eq. 11A.

$$\frac{A_2R_2'}{A^0} = \left[\frac{k_R[R^0]}{\tau_\alpha^{-1} - \tau_\beta^{-1}}\right]^2 \left[\frac{[A^0]}{2[R^0]}\right] [e^{-2t/\tau_\beta} + e^{-2t/\tau_\alpha} - 2e^{-t/(\tau_\alpha^{-1}+\tau_\beta^{-1})}]. \quad (11A)$$

The postulate of receptor site independence in scheme III is reflected in Eqs. 10A and 11A by the relationship $[A_2R_2']/[R^0] = ([AR']/[R^0])^2/2$, as expected from a simple probability argument. The time t_p to peak binding of acetylcholine is obtained by differentiating Eq. 7A with respect to t and is given by Eq. 12A.

$$t_p = \frac{\ln(\tau_\beta/\tau_\alpha)}{\tau_\alpha^{-1} - \tau_\beta^{-1}}. \quad (12A)$$

APPENDIX II

Simulation Assuming Two Reaction Spaces

Simulations of epcs were conducted on a TR-20 analog computer (Electronic Associates, Inc., West Long Branch, N.J.) and displayed on an x-y recorder. The complete array of differential equations which correspond to the two-reaction space model are given in Eqs. 13A–19A.

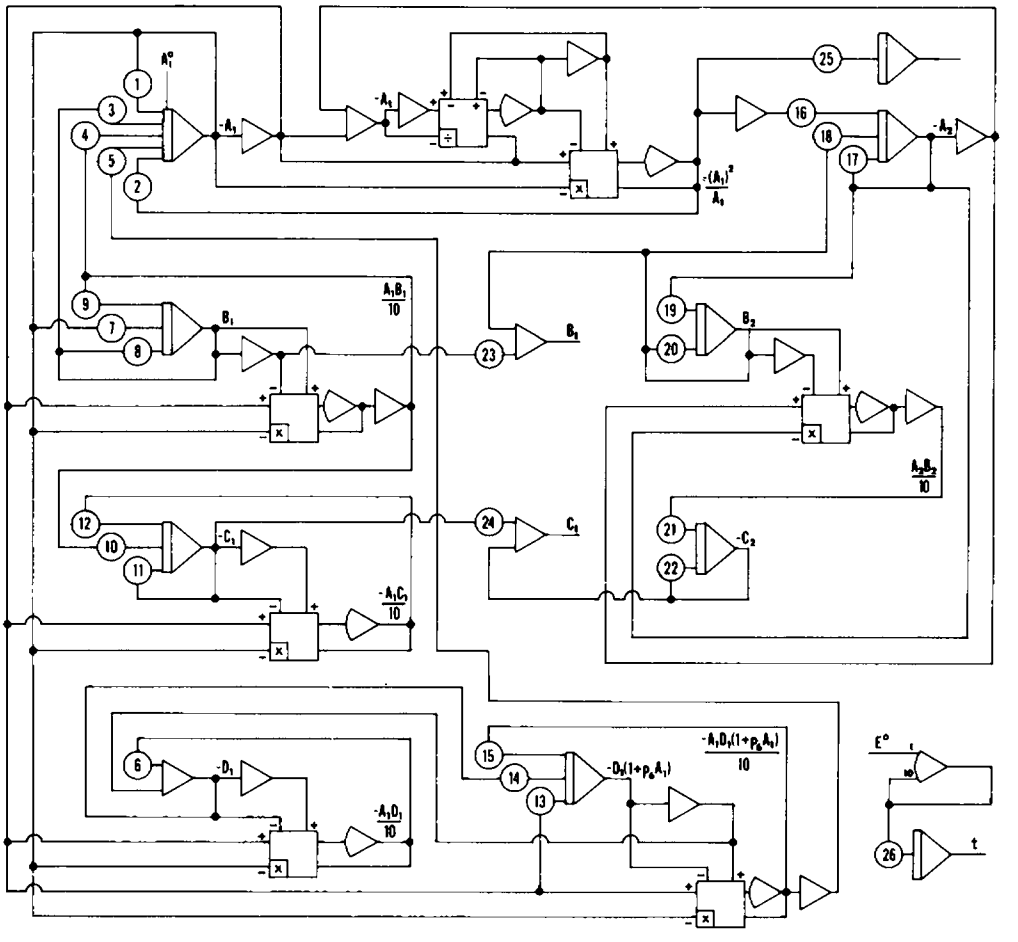

FIGURE 7 Analog computer circuit diagram for the two-reaction space model. The initial condition was $A_1^0 = 10$ V. The recorder time base input voltage E^0 was 10 V throughout.

$$\frac{dA_1}{dt} = -p_1A_1 - p_2\frac{(A_1)^2}{A_t} + p_3B_1 + p_4A_1B_1 + p_5A_1D_1(1 + p_6A_1) \quad (13A)$$

$$-\frac{dB_1}{dt} = -p_7A_1 + p_8B_1 + p_9A_1B_1 \quad (14A)$$

$$\frac{dC_1}{dt} = p_{10}A_1B_1 - p_{11}C_1 - p_{12}A_1C_1 \quad (15A)$$

$$\frac{d[D_1(1 + p_6A_1)]}{dt} = p_{13}A_1 - p_{14}D_1 - p_{15}A_1D_1(1 + p_6A_1) \quad (16A)$$

$$\frac{dA_2}{dt} = p_{16}\frac{(A_1)^2}{A_t} - p_{17}A_2 + p_{18}B_2 \quad (17A)$$

$$-\frac{dB_2}{dt} = -p_{19}A_2 + p_{20}B_2 \quad (18A)$$

$$\frac{dC_2}{dt} = p_{21}A_2B_2 - p_{22}C_2. \quad (19A)$$

These equations were programmed according to the circuit diagram in Fig. 7. The capitalized circuit symbols in the equations are variables defined in Table III. The p terms are constants defined in Table IV, where the values of the constants used in the simulations in Fig. 4 are displayed. For the homogeneous reaction space model, only Eqs. 17A–19A apply with $p_{16} = 0$ and the initial condition $A_2^0 = 10$ V.

This work was greatly stimulated by initial helpful discussions with Dr. Eberhard Neumann, Max-Planck-Institute for Biochemistry, Martinsried near Munich, West Germany and was carried out with an analog computer kindly provided by Dr. Martin Blank, Department of Physiology, Columbia University.

TABLE III
RELATIONSHIP BETWEEN ANALOG COMPUTER VOLTAGES AND CHEMICAL SPECIES

Circuit symbol	Definition	Scaling factor	Value of scaling factor*
Volts	*Volts*		*Volts* · m^{-1}
A_2	$a_2[A]_{II}$	a_2	6.67×10^5
B_2	$b_2[AR']_{II}$	b_2	a_2
C_2	$c_2[A_2R_2']_{II}$	c_2	$5a_2$
A_1	$a_1[A]_I$	a_1	V_Ia_2/V_T
B_1	$b_1[AR']_I$	b_1	$2V_Ia_2/V_T$
C_1	$c_1[A_2R_2']_I$	c_1	$5V_Ia_2/V_T$
D_1	$d_1[acE]_I$	d_1	$5V_Ia_2/V_T$
			Volts · mol^{-1}
A_t	$a_TA_T = a_1[A]_I + a_2[A]_{II}$	a_T	a_2/V_T
B_t	$b_TAR_T' = b_1p_{23}[AR']_I + b_2[AR']_{II}$	b_T	a_2/V_T
C_t	$c_TA_2R_{2T}' = c_1p_{24}[A_2R_2']_I + c_2[A_2R_2']_{II}$	c_T	$5a_2/V_T$

*These values include the approximation $V_{II} \simeq V_T$, where V_I, V_{II}, and V_T are the respective volumes of the first, the second, and the total reaction spaces.

TABLE IV
VALUES OF ANALOG COMPUTER SETTINGS
USED IN THE SIMULATIONS IN FIG. 4

Circuit symbol p	Definition	Value in computer time*	
		Full $[E]$	$[E^0]_T = 0$
1	$k_R[R^0]_I + k_E[E^0]_I$	4.5 s^{-1}	1.5 s^{-1}
2	k_0	2.1 s^{-1}	2.1 s^{-1}
3	$a_1 k_{-R}/b_1$	0.05 s^{-1}	0.05 s^{-1}
4	$10\,k_R/b_1$	1.5 $volt^{-1}\,s^{-1}$	1.5 $volt^{-1}\,s^{-1}$
5	$10\,k_E/d_1$	6.0 $volt^{-1}\,s^{-1}$	6.0 $volt^{-1}$
6	$10/a_1[A^0]_I$‡	1.0 $volt^{-1}$	1.0 $volt^{-1}$
7	$b_1 k_R[R^0]_I/a_1$	3.0 s^{-1}	3.0 s^{-1}
8	k_{-R}	0.1 s^{-1}	0.1 s^{-1}
9	$10\,k_R/a_1$	3.0 $volt^{-1}\,s^{-1}$	3.0 $volt^{-1}\,s^{-1}$
10	$10\,c_1 k_R/a_1 b_1$	7.5 $volt^{-1}\,s^{-1}$	7.5 $volt^{-1}\,s^{-1}$
11	$2k_{-R}$	0.2 s^{-1}	0.2 s^{-1}
12	$20\,k_R/a_1$	6.0 $volt^{-1}\,s^{-1}$	6.0 $volt^{-1}\,s^{-1}$
13	$d_1 k_E[E^0]_I/a_1$	15.0 s^{-1}	0
14	k_3^E	3.0 s^{-1}	3.0 s^{-1}
15	$10\,k_E/a_1$	30.0 s^{-1}	30.0 s^{-1}
16	k_0	2.1 s^{-1}	2.1 s^{-1}
17	$k_R[R^0]_{II} + k_E[E^0]_{II} + k_D$	3.42 s^{-1}	0.42 s^{-1}
18	$a_2 k_{-R}/b_2$	0.10 s^{-1}	0.10 s^{-1}
19	$b_2 k_R[R^0]_{II}/a_2$	0.30 s^{-1}	0.30 s^{-1}
20	k_{-R}	0.1 s^{-1}	0.1 s^{-1}
21	$10\,c_2 k_R/a_2 b_2$	0.30 $volt^{-1}\,s^{-1}$	0.30 $volt^{-1}\,s^{-1}$
22	$2\,k_{-R}$	0.2 s^{-1}	0.2 s^{-1}
23	$b_2 V_1/b_1 V_T$	0.5 (dimensionless)	0.5 (dimensionless)
24	$c_2 V_1/c_1 V_T$	1.0 (dimensionless)	1.0 (dimensionless)
25	k_0	2.1 s^{-1}	2.1 s^{-1}
26	Recorder time base	0.5 s^{-1}	0.5 s^{-1}

*Computer time is obtained by multiplying real time by 5,000. The feedback capacitance for integrators is 10 μF, and thus the input resistance R for each integrator input is $1/(p)(10\ \mu F)$ (e.g., for p_1, R_1 = 22.2 KΩ; this R_1 is achieved by coupling a grounded potentiometer at setting 0.45 to a 10 KΩ input resistor). The feedback resistance for inverting and summing amplifiers is 100 KΩ, and thus the input resistance R for each inverting and summing input is $1/(p)$(100 KΩ) (e.g., for p_{23}, R_{23} = 200 KΩ).

‡This definition assumes that $K_i = [A^0]_I$. In most simulations (unless otherwise noted), substrate inhibition was assumed negligible, and p_6 was set equal to zero.

The research was supported by grants from the National Science Foundation, NSF-PCM77-09383, and the U.S. Public Health Service, NS-11766.

Received for publication 24 July 1978 and in revised form 29 November 1978.

REFERENCES

ADAMS, P. R. 1975. An analysis of the dose-response curve at voltage-clamped frog endplates. *Pflügers Arch. Eur. J. Physiol.* **360**:145–153.

ALDRIDGE, W. N., and E. REINER. 1969. Acetylcholinesterase. Two types of inhibition by an organophosphorus compound: one the formation of phosphorylated enzyme and the other analogous to inhibition by substrate. *Biochem. J.* **115**:147–162.

ANDERSON, C. R., and C. F. STEVENS. 1973. Voltage clamp analysis of acetylcholine produced end-plate current fluctuations at frog neuromuscular junction. *J. Physiol. (Lond.).* **235**:655–691.

BARNARD, E. A., T. RYMASZEWSKA, and J. WIECKOWSKI. 1971. Cholinesterases at individual neuromuscular junctions. *In* D. J. Triggle, J. F. Moran, and E. A. Barnard, editors. Cholinergic Ligand Interactions. Academic Press Inc., New York. 175–200.

BOURGEOIS, J. P., A. RYTER, A. MENEZ, P. FROMAGEOT, P. BOQUET, and J.-P. CHANGEUX, 1972. Localization of the cholinergic receptor protein in *Electrophorus* electroplax by high resolution autoradiography. *FEBS (Fed. Eur. Biochem. Soc.) Lett.* **25**:127–133.

CHANG, H. W., and E. BOCK. 1977. Molecular forms of acetylcholine receptor. Effects of calcium ions and a sulfhydryl reagent on the occurrence of oligomers. *Biochemistry.* **16**:4513–4520.

CHANGEUX, J-P., J. THIÉRY, Y. TUNG, and C. KITTEL. 1967. On the cooperativity of biological membranes. *Proc. Natl. Acad. Sci. U. S. A.* **57**:335–341.

COLQUHOUN, D. 1975. Mechanisms of drug action at the voluntary muscle endplate. *Annu. Rev. Pharmacol.* **15**:307–320.

CRANK, J. 1957. The Mathematics of Diffusion. Oxford University Press, London. 27–28.

DAMLE, V. N., and A. KARLIN. 1978. Affinity labelling of one of two α-neurotoxin binding sites in acetylcholine receptor from *Torpedo californica*. *Biochemistry.* **17**:2039–2045.

DEL CASTILLO, J., and B. KATZ. 1957. Interaction at end-plate receptors between different choline derivatives. *Proc. R. Soc. Lond. B. Biol. Sci.* **146**:369–381.

DOWDALL, M. J., G. FOX, K. WAECHTLER, V. P. WHITTAKER, and H. ZIMMERMANN. 1976. Recent studies on the comparative biochemistry of the cholinergic neuron. *Cold Spring Harbor Symp. Quant. Biol.* **40**:65–81.

ECCLES, J. C., and J. C. JAEGER. 1958. The relationship between the mode of operation and the dimensions of the junctional region at synapses and motor end-organs. *Proc. R. Soc. B.* **148**:38–56.

EIGEN, M., and L. DE MAEYER. 1963. Relaxation methods. *Tech. Org. Chem.* **8** (part 2):895–1054.

FAMBROUGH, D. M., and H. C. HARTZELL. 1972. Acetylcholine receptors: number and distribution at neuromuscular junctions in rat diaphragm. *Science (Washington, D.C.).* **176**:189–191.

FERTUCK, H. C., and M. M. SALPETER. 1976. Quantitation of junctional and extrajunctional acetylcholine receptors by electron microscope autoradiography after ^{125}I-α-bungarotoxin binding at mouse neuromuscular junctions. *J. Cell Biol.* **69**:144–158.

GAGE, P. W., and R. N. MCBURNEY. 1975. Effects of membrane potential, temperature and neostigmine on the conductance change caused by a quantum of acetylcholine at the toad neuromuscular junction. *J. Physiol. (Lond.).* **244**:385–407.

GRÜNHAGEN, H-H., M. IWATSUBO, and J-P. CHANGEUX. 1977. Fast kinetic studies on the interaction of cholinergic agonists with the membrane-bound acetylcholine receptor from *Torpedo marmorata* as revealed by quinacrine fluorescence. *Eur. J. Biochem.* **80**:225–242.

HARTZELL, H. C., S. W. KUFFLER, and D. YOSHIKAMI. 1975. Post-synaptic potentiation: interaction between quanta of acetylcholine at the skeletal neuromuscular synapse. *J. Physiol. (Lond.).* **251**:427–463.

KARLIN, A. 1967. On the application of "a plausible model" of allosteric proteins to the receptor for acetylcholine. *J. Theor. Biol.* **16**:306–320.

KATZ, B. 1969. The Release of Neural Transmitter Substances. Charles C. Thomas, Springfield, Ill. 60.

KATZ, B., and R. MILEDI. 1965. The measurement of synaptic delay, and the time course of acetylcholine release at the neuromuscular junction. *Proc. R. Soc. Lond. B. Biol. Sci.* **161**:483–496.

KATZ, B., and R. MILEDI. 1972. The statistical nature of the acetylcholine potential and its molecular components. *J. Physiol. (Lond.).* **224**:665–699.

KATZ, B., and R. MILEDI. 1973. The binding of acetylcholine to receptors and its removal from the synaptic cleft. *J. Physiol. (Lond.).* **231**:549–574.

KORDAS, M. 1972*a*. An attempt at an analysis of the factors determining the time course of the end-plate current. I. The effects of prostigmine and the ratio of Mg^{++} to Ca^{++}. *J. Physiol. (Lond.).* **224**:317–332.

KORDAS, M. 1972*b*. An attempt at an analysis of the factors determining the time course of the end-plate current. II. Temperature. *J. Physiol. (Lond.).* **224**:333–348.

KRUPKA, R. M., and K. J. LAIDLER. 1961. Molecular mechanisms for hydrolytic enzyme action. I. Apparent non-competitive inhibition, with special reference to acetylcholinesterase. *J. Am. Chem. Soc.* **83**:1445–1460.

KUFFLER, S. W., and D. YOSHIKAMI. 1975. The number of transmitter molecules in a quantum: an estimate from iontophoretic application of acetylcholine at the neuromuscular synapse. *J. Physiol. (Lond.).* **251**:465–482.

LESTER, H. A., J-P. CHANGEUX, and R. E. SHERIDAN. 1975. Conductance increases produced by bath application of cholinergic agonists to *Electrophorus* electroplaques. *J. Gen. Physiol.* **65**:797–816.

LESTER, H. A., D. D. KOBLIN, and R. E. SHERIDAN. 1978. Role of voltage-sensitive receptors in nicotinic transmission. *Biophys. J.* **21**:181–194.

MAGLEBY, K. L., and C. F. STEVENS. 1972*a*. The effect of voltage on the time course of end-plate currents. *J. Physiol. (Lond.)*. **223**:151–171.

MAGLEBY, K. L., and C. F. STEVENS. 1972*b*. A quantitative description of end-plate currents. *J. Physiol. (Lond.)*. **223**:173–197.

MAGLEBY, K. L., and D. A. TERRAR. 1975. Factors affecting the time course of decay of end-plate currents: a possible cooperative action of acetylcholine on receptors at the frog neuromuscular junction. *J. Physiol. (Lond.)*. **244**:467–495.

MATTHEWS-BELLINGER, J., and M. M. SALPETER. 1978. Distribution of acetylcholine receptors at frog neuromuscular junctions with a discussion of some physiological implications. *J. Physiol. (Lond.)*. **279**:197–213.

MILEDI, R., and L. T. POTTER. 1971. Acetylcholine receptors in muscle fibers. *Nature (Lond.)*. **233**:599–603.

MITCHELL, J. F., and K. KRNJEVIĆ. 1961. The release of acetylcholine in the isolated rat diaphragm. *J. Physiol. (Lond.)*. **155**:246–262.

NACHMANSOHN, D. 1955. Metabolism and function of the nerve cell. Harvey Lect. **49**:57–99.

NACHMANSOHN, D. 1959. Chemical and Molecular Basis of Nerve Activity. Academic Press Inc., New York. 325; revised (1975), 403.

NACHMANSOHN, D., and I. B. WILSON. 1951. The enzymic hydrolysis and synthesis of acetylcholine. *Adv. Enzymol.* **12**:259–339.

NEGRETE, J., J. DEL CASTILLO, I. ESCOBAR, and G. YANKELEVICH. 1972. Correlation between amplitudes and rise times of the miniature endplate potentials in frog muscle. *Int. J. Neurosci.* **4**:1–10.

NEUMANN, E., and H. W. CHANG. 1976. Dynamic properties of isolated acetylcholine receptor protein: kinetics of the binding of acetylcholine and Ca ions. *Proc. Natl. Acad. Sci. U. S. A.* **73**:3994–3998.

NEUMANN, E., D. NACHMANSOHN, and A. KATCHALSKY. 1973. An attempt at an integral interpretation of nerve excitability. *Proc. Natl. Acad. Sci. U. S. A.* **70**:727–731.

NEUMANN, E., T. L. ROSENBERRY, and H. W. CHANG. 1978. Elementary chemical reactions of acetylcholine with receptor and esterase. Relationship to neuronal information transfer. *In* Neuronal Information Transfer. A. Karlin, V. M. Tennyson, and H. J. Vogel, editors, Academic Press Inc., New York. 183–210.

PEPER, K., F. DREYER, and K-D. MÜLLER. 1976. Analysis of cooperativity of drug-receptor interaction by quantitative iontophoresis at frog motor end plates. *Cold Spring Harbor Symp. Quant. Biol.* **40**:187–192.

PERRIN, C. L. 1970. Mathematics for Chemists. Wiley-Interscience, John Wiley & Sons, New York. 281–282.

PORTER, C. W., T. H. CHIU, J. WIECKOWSKI, and E. A. BARNARD. 1973. Types and locations of cholinergic receptor-like molecules in muscle fibers. *Nat. New Biol.* **241**:3–7.

POTTER, L. T. 1970. Synthesis, storage and release of C^{14} acetylcholine in isolated rat diaphragm muscles. *J. Physiol. (Lond.)*. **206**:145–166.

RAFTERY, M. A., R. L. VANDLEN, K. L. REED, and T. LEE. 1976. Characterization of *Torpedo californica* acetylcholine receptor: its subunit composition and ligand-binding properties. *Cold Spring Harbor Symp. Quant. Biol.* **40**:193–202.

RANG, H. P. 1975. Acetylcholine receptors. *Q. Rev. Biophys.* **7**:283–400.

ROSENBERRY, T. L. 1975. Acetylcholinesterase. *Adv. Enzymol.* **43**:103–218.

ROSENBERRY, T. L., and S. A. BERNHARD. 1972. Studies of catalysis by acetylcholinesterase. Synergistic effects of inhibitors during the hydrolysis of acetic acid esters. *Biochemistry.* **11**:4309–4321.

SALPETER, M. M., and M. E. ELDEFRAWI. 1973. Sizes of end plate compartments, densities of acetylcholine receptor and other quantitative aspects of neuromuscular transmission. *J. Histochem. Cytochem.* **21**:769–778.

SHERIDAN, R. E., and H. A. LESTER. 1977. Rates and equilibria at the acetylcholine receptor of *Electrophorus* electroplaques. *J. Gen. Physiol.* **70**:187–219.

STEINBACH, J. H., and C. F. STEVENS. 1976. Neuromuscular transmission. *In* R. Llinas and W. Precht, editors. Frog Neurobiology. Springer Verlag-New York. 33–92.

TAKEUCHI, A., and N. TAKEUCHI. 1959. Active phase of frog's end-plate potential. *J. Neurophysiol.* **22**:395–411.

WILSON, I. B., and E. CABIB. 1956. Acetylcholinesterase: enthalpies and entropies of activation. *J. Am. Chem. Soc.* **78**:202–207.